# Auger decay of the 3 d hole in the isoelectronic series of Br, Kr + , and Rb 2 +

J. Keskinen, K. Jänkälä, S.-M. Huttula, T. Kaneyasu, Y. Hikosaka, E. Shigemasa, H. Iwayama, K. Soejima, K. Ito, L. Andric, et al.

# Auger decay of the $3d$ hole in the isoelectronic series of $Br^*$, $Kr^+$ and $Rb^{2+}$

J. Keskinen,[1,*] K. Jänkälä,[1] S.-M. Huttula,[1] T. Kaneyasu,[2] Y. Hikosaka,[3] E. Shigemasa,[4] H. Iwayama,[4] K. Soejima,[5] K. Ito,[6] L. Andric,[7] M. Khalal,[7] J. Palaudoux,[7] F. Penent,[7] and P. Lablanquie[7]

[1] *Nano and Molecular Systems Research Unit, University of Oulu, P.O. Box 3000, 90014 Oulu, Finland*
[2] *SAGA Light Source, Tosu 841-0005, Japan*
[3] *Institute of Liberal Arts and Sciences, University of Toyama, Toyama 930-0194, Japan*
[4] *Institute for Molecular Science, Okazaki 444-8585, Japan*
[5] *Department of Environmental Science, Niigata University, Niigata 950-2181, Japan*
[6] *Synchrotron SOLEIL, l'Orme des Merisiers, Saint-Augin, BP 48, 91192 Gif-sur-Yvette Cedex, France*
[7] *Sorbonne Université, CNRS, Laboratoire de Chimie Physique-Matiére et Rayonnement, 4 place Jussieu, 75005 Paris, France*

(Dated: October 2, 2019)

The Auger decays following the $3d$ hole state in configuration $[\mathrm{Ar}]\,3d^{-1}4s^24p^6$ of the isoelectronic series $Br^*$, $Kr^+$, and $Rb^{2+}$ were studied through multielectron coincidence methods. In addition, the decays of the $3d_{5/2}$ and $3d_{3/2}$ hole states in $Br^*$ could also be separated with traditonal methods by utilizing the $\sigma^*$ resonance in HBr. Coincidence methods were used to further study specific details of the decays, evolution of spectral features and binding energies within the isoelectronic series, as well as in the case of $Br^*$ to look into the subsequent *normal* super-Coster-Kronig type $NNN$ Auger decay into the doubly ionized $Br^{2+}$ states. Interpretation was done with the aid of multiconfiguration Dirac-Fock calculations.

PACS numbers: 32.80.Hd, 32.80.Fb

## I. INTRODUCTION

Shallow inner-shell atomic holes are excited states that decay dominantly by release of a so called 'Auger electron', in reference to its description by P. Auger in 1925 [1]. However a weaker, 'double Auger' path, in which two Auger electrons are emitted was discovered at the end of the 60's in rare gas atoms Ne and Ar [2, 3]. The advent of coincidence experiments brought deeper insight revealing that the double Auger path can proceed through a series of decays called cascade decays [4–7]. The direct double Auger decay in which the two Auger electrons are simultaneously emitted is, on the other hand, a fascinating manifestation of a true three electron correlation process. Its detailed study took more time, both by experiment [5] and by theory, which refers to knock-out and shake-off mechanisms to describe it [8, 9]. Experimental evidence for a direct triple Auger decay has also been found in Ar [10].

In this work, we have studied the Auger decays of $3d$ hole in the isoelectronic configuration $[\mathrm{Ar}]\,3d^94s^24p^6$ of $Br^*$, $Kr^+$ and $Rb^{2+}$. The singly ionized $Kr^+$ $3d^94s^24p^6$ ion goes through an $M_{4,5}NN$ Auger decay, which has been studied extensively over the time of five decades [7, 11–15]. These studies have, among other things, shown that the $3d$ photoionization of Kr is followed by a cascade Auger decay, and thus a similar behavior can be expected to follow the $3d$ excitation in atomic Br and ionic $Rb^{2+}$. Previous experiments on absorption [16] and on-resonance photoelectron spectroscopy as well as theoretical study of $3d \rightarrow 4p$ excited Br have indeed provided convincing evidence for this [17]. The linewidths have been best explained by theory when further decay into singly ionized $Br^+$ states has been assumed dominant [18].

As bromine is highly reactive in atomic form, we prepared the $Br^*$ $3d^{-1}4s^24p^6$ states by ultrafast dissociation of the HBr molecule upon $3d_{5/2} \rightarrow \sigma^*$ excitation [19]. The observed process in Br can be described with the following equation

$$\mathrm{h}\nu + \mathrm{HBr} \rightarrow \mathrm{HBr}\,(3d \rightarrow \sigma^*) \rightarrow \mathrm{H} + \mathrm{Br}\,(3d^{-1}4p^6) \rightarrow \mathrm{Br}^+ + \epsilon^-$$

in which $\mathrm{h}\nu$ is the photon which excites the target molecule and $\epsilon^-$ is the electron ejected from the system as a result of a resonant Auger process.

The Auger decays have been measured using synchrotron radiation and interpreted with theoretical predictions obtained from multiconfiguration Dirac-Fock calculations. The possibility to theoretically simulate the following second step Auger process and to use the data obtained from Auger electron-Auger electron coincidence studies (e.g. the extracted on- and off-resonance double photoionization spectra) enabled even more detailed analysis of the Auger decay of $3d$ hole in $Br^*$ and its comparison with $Kr^+$ and $Rb^{2+}$ atoms.

## II. EXPERIMENT

The study used two experimental setups: first, a multielectron coincidence spectrometer, the magnetic bottle time-of-flight spectrometer HERMES [7, 10]. It provides an energy resolution $\Delta E/E$ of ∼1.6%, where E is the kinetic energy of the electron. Second, a high-resolution hemispherical electron energy analyzer (MBS-A1) [20]. Its resolution was $\Delta E$ 20 meV, including the contribution of the analyzer (12 meV) and of the Doppler broadening

* juho.keskinen@oulu.fi

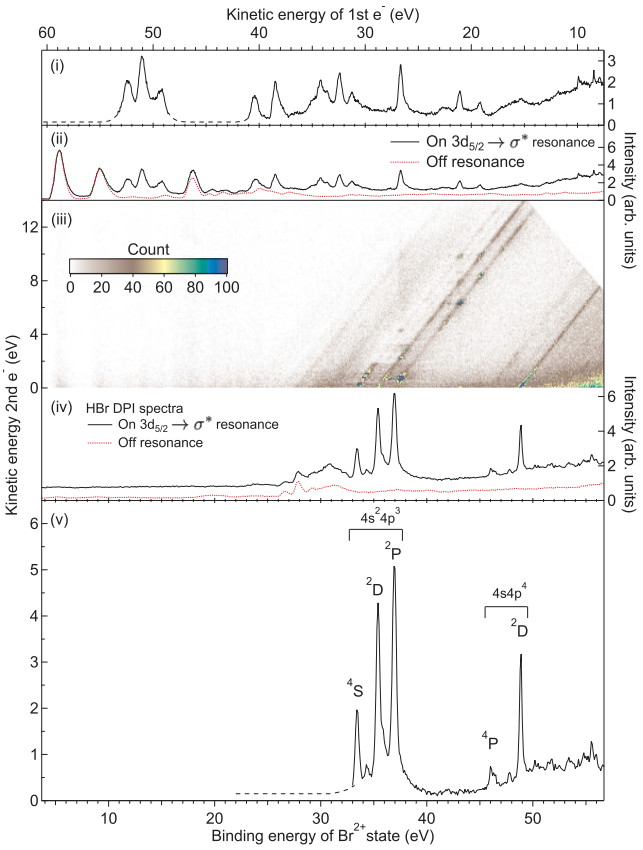


FIG. 1. The frame **(iii)** represents the collected Auger electron-Auger electron coincidence map after the $3d_{5/2} \rightarrow \sigma^*$ resonance in HBr. The recorded electron counts are denoted by colors. The **(ii)** frame depicts the results of vertical integration of the map as a solid line, which represents the Auger decay of atomic Br* following the $3d_{5/2} \rightarrow \sigma^*$ resonance at 70.7 eV as well as wider lines corresponding to HBr molecule. The dotted (red) line shows the off-resonance measurement at 75.3 eV (shifted 4.4 eV lower in binding energy) and features only molecular lines. The **(i)** frame features the decay spectrum with the molecular contribution subtracted. The **(iv)** frame shows the double photoionization (DPI) spectrum measured on the HBr $3d_{5/2} \rightarrow \sigma^*$ resonance (solid) extracted from the map by integrating diagonally along total excess energy as well as a comparison with the corresponding spectrum collected off resonance (dotted) at $h\nu = 75.3\ eV$. The **(v)** frame shows the DPI spectrum with the molecular (off-resonance) contribution subtracted; labels denote the main contributing configuration of the linegroups. The spectra are aligned with the map and presented in the binding energy of the $Br^{2+}$ state (bottom axis) as well as the kinetic energy of the faster detected electron (top axis).

(10 meV). The axis of the electrostatic lens of the analyzer was perpendicular to the photon beam and fixed at the magic angle (54.7°) relative to the direction of polarization of the incident synchrotron radiation.

The experiments on Kr and Rb were performed at the undulator beamline PLEIADES [21] of the SOLEIL synchrotron facility during the single bunch operating mode of the synchrotron, providing bunches of light every 1184 ns. The Auger decay of the $Kr^+$ $3d^{-1}4s^24p^6$ states were obtained by analyzing coincidences with a $3d$ photoelectron, in a similar way as was done by Palaudoux et al [7]. The Auger decay of the $Rb^{2+}$ $3d^{-1}4s^24p^6$ states involved a more complex analysis, in which the Auger electrons are identified by their detection in coincidence with the pair of $3d$ and $5s$ photoelectrons. Such a procedure was developed to study the Auger decay of the $Ar^{2+}$ $2p^{-1}3s^23p^5$ states [22] and applied in the study of the decay of the $4d$ hole in the $Xe^+$ ion [23].

The excited Br $3d^{-1}4s^24p^6$ state was created through ultra-fast dissociation of HBr molecule upon $3d \rightarrow \sigma^*$ excitation [19]. Its Auger decay was obtained using the multielectron coincidence setup HERMES at the undulator beam line U56/2 PGM2 [24] of the BESSY-II synchrotron radiation facility in Berlin, Germany. The synchrotron was used in its single-bunch operation mode, providing bunches of light every 800.5 ns. Fig. 1 displays the Auger spectra measured at the HBr $3d_{5/2} \rightarrow \sigma^*$ resonance. The raw spectra contain the contribution of the multiple ionization of the HBr molecule. The Auger decay of the atomic Br $3d^{-1}4s^24p^6$ state is obtained by subtracting an off-resonance spectrum. This is illustrated in the (ii) frame of Fig. 1, in which the on- and off-resonance, total 1-dimensional Auger spectra are shown. The difference gives the atomic component, and is displayed in the (i) frame of Fig. 1. In a similar way the raw 2-dimensional energy correlation map of electron-electron coincidences measured at the $3d_{5/2} \rightarrow \sigma^*$ resonance is displayed in the (iii) frame Fig. 1. Integration along the diagonal lines gives the final dicationic states shown in the frame (iv) of Fig. 1. The contribution associated to the double ionization of the HBr molecule is estimated off-resonance. Its subtraction gives in the (v) frame of Fig. 1 the population of the $Br^{2+}$ states populated upon double Auger decay of the Br $3d_{5/2}^{-1}4s^24p^6$ state.

Finally a high resolution conventional Auger spectrum of the Br $3d^{-1}4s^24p^6$ state was obtained with the MBS-A1 analyzer at the soft X-ray beamline BL6U at the UVSOR facility in the Institute for Molecular Science in Okazaki, Japan [20]. The $j = 5/2$ component of the measured spectrum of Br is presented in the upper panel in Fig. 2.

## III. CALCULATIONS

Theoretical simulation of the $3d$ hole decay process was carried out using the multiconfiguration Dirac-Fock (MCDF) method with the flexible atomic code (FAC) [25] as well as the atomic structure code GRASP2K [26, 27] to acquire theoretical predictions for the decays in the studied isoelectronic series. The atomic state functions (ASF) were acquired by diagonalizing the Hamiltonian matrix in the basis of $jj$-coupled antisymmetric configuration state functions (CSF) of the same total angular momentum and parity. Finally the ASF mixing coeffi-

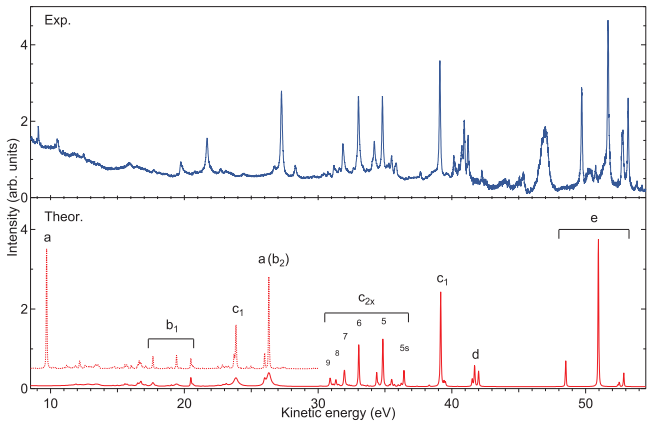


FIG. 2. The measured and simulated resonant Auger spectra resulting from the decay of the Br* $3d_{5/2}^{-1}$ state. The dotted line represent simulated spectra without the contribution of the subsequent decay. Labels correspond to the different contributing configurations in the following manner; **a**: $4p^6$, $\mathbf{b}_1$: $4s4p^4(5s, 6/7/9d)$, $\mathbf{b}_2$: $4s4p^4 4d$, $\mathbf{c}_1$: $4s^2 4p^3 4d$, $\mathbf{c}_{2x}$: $4s^2 4p^3(5s, nd)$, **d**: $4s4p^5$, **e**: $4s^2 4p^4$. Bracketed labels correspond to configurations that strongly mix with the main contributing configurations. In the case of $\mathbf{c}_{2x}$ additional $n/n\ell$ labeling marked above the corresponding peaks defines the configuration in more detail.

cients and the state energies were determined and the Auger decay matrix elements determined.

In each of the isoelectronic cases the simulation with FAC was run in two parts; the first part featuring the initial decay of the $3d$ hole state into the intermediate states, and the second part featuring the subsequent Auger decay of those intermediate states into their final states. During the first part of the simulation the nonrelativistic configuration $3d^9 4s^2 4p^6$ is used to describe the initial $3d$ hole state. The final states of the first part (intermediate states) are described by a set of nonrelativistic configurations, which are $4p^6$, $4s^2 4p^4$, $4p^4(5s, 4/5/6d)^2$, $4p^4 4d\,kd$, $4s4p^4(5s, md)$, $4/5s\,np^5$, $np^5 md$, $4s^2 np^3(5s, md)$, $4s^2 4p^2 \ell p(5s, md)$, $4s^2 4p\,\ell p^2(5s, md)$, $4/5s\,4p^4 \ell p$, $4/5s\,4p\,\ell p^4$, $4p^4 \ell p\,md$, $4p\,\ell p^4 md$, $4/5s\,4p^3 \ell p^2$, and $4p^3 \ell p^2 md$, in which $n = 4, 5, 6, 7, 8$; $m = 4, 5, 6, 7, 8, 9$; $\ell = 5, 6, 7, 8$; and $k = 5, 6, 7, 8, 9$. The simulation of the decay into the states consisting of these configurations was run separately for even and odd parity cases.

The simulation of the subsequent Auger decay was performed in order to obtain theoretical estimates for the lifetimes of the intermediate states namely the final states of the first step in the decay process. The second part features the large set of intermediate states describing its initial states, whereas the final states consist of the nonrelativistic configurations $4s^2 4p^3$, $4s^2 4p^2(5s, 4/5d)$, $4s^2 4p(5s^2, 4/5d^2, 4d5d)$, $4s\,4p^4$, $4s\,4p^3(5s, 4/5d)$, $4s\,4p^2(5s^2, 4/5d^2, 4d5d)$, $4p^5$, $4p^4(5s, 4/5d)$, and $4p^3(5s^2, 4/5d^2, 4s5d)$. The calculated lifetimes contribute to the width of the peaks observed in the Auger spectrum seen in Fig. 2. Statistical weights were assumed for the initial $3d_j$ hole states.

In order to get a more comprehensive understanding of the underlying processes, they were also simulated with GRASP2K and the associated RATIP suite [28, 29], which has the components RELCI and AUGER for determining the mixing coefficients and decay matrix elements respectively. Because of the limitations imposed by the code and to achieve convergence, a more limited set of nonrelativistic configurations was used. The initial $3d$ hole state was described by the configuration $3d^9 4s^2 4p^6$, and the intermediate states consists of configurations $4p^6$, $4s^2 4p^4$, $4s^2 4p^4(5s, 4/5/6d)$, $4s^2 4p^2(4d^2, 5s^2, 4d5d)$, $4s4p^5$, and $4s^2 4p^3(5s, 4/5d)$. The states of the final step were described by a set of configurations, which are $4s^2 4p^3$, $4s^2 4p^2(5s, 4/5/6d)$, $4s4p^4$, $4s4p^3 4d$, $4s4p^2 4d^2$, and $4p^5$.

## IV. DISCUSSION

The Auger spectra of the decay of the $3d$ hole in the isoelectronic series of atomic Br*, $Kr^+$, and $Rb^{2+}$ bear resemblances to each other, but interestingly also notable differences. We will show that the evolution of various identified, equivalent linegroups and total intensity distribution within the series can be followed as a function of the atomic number $Z$. All the studied intermediate and final atomic states in the series are very sensitive to configuration mixing in the MCDF scheme, which is the reason for some of the discrepancies in labeling in contrast with some earlier studies [7, 14] as well as within the series regarding the leading configuration. The resonant Auger spectrum of Br* has the visually richest linestructure and as one especially interesting feature, which sets it apart from its isoelectronic counterparts. Therefore it will be separately discussed later in this section.

We will first describe the processes following the resonant Auger decay in Br* in detail comparing it with earlier studies on the isoelectronic $Kr^+$ [7, 14], after which we will describe the trends observable in the isolectronic series of Br*, $Kr^+$, and $Rb^{2+}$.

### A. Resonant Auger decay in Br

The $j = 5/2$ component of the resonant Auger spectrum collected with the hemispherical electron energy analyzer (MBS-A1) at BL6U is presented with a solid blue line in Fig. 2 as a function of the kinetic energy of the ejected Auger electron. The lower panel shows a theoretical prediction as a solid red line obtained from FAC.

Starting from at around 39 eV in the collected spectra (see the upper panel of Fig. 2) the equivalents of the linegroups $\mathbf{c}_1$, **d**, and **e** in the order of ascending kinetic energy can be found relatively easily in the $Kr^+$ $3d$ hole decay spectra (see Refs. [7, 14]). The resonant Auger spectra features also wide lines arising from the molecular

HBr from energies 40 eV onwards, which makes objective comparison of the individual line or even linegroup intensities somewhat challenging. Despite this it is possible to see that the total intensity of the decay in Br* is more evenly distributed among the observed lines than in the case of its $Kr^+$ counterpart. Besides the apparent lower intensity of the observed lines in the kinetic energy range of 31 to 38 eV (designated as $\mathbf{c}_{2x}$ in Fig. 2), the linestructure itself in this region also appears significantly richer in Br*. Theoretical inspection reveals that the series of lines seen within $\mathbf{c}_{2x}$ arise from decay into the final states of the resonant Auger decay in which either $5s$, $5d$, $6d$, $7d$, $8d$, or $9d$ orbital (in the order of descending kinetic energy) is singly occupied in the main contributing configuration, namely $4s^24p^3(5s, 5d, 6d, 7d, 8d, 9d)$. On the lower energy side of $\mathbf{c}_{2x}$ we have two linegroups $\mathbf{a(b}_2\mathbf{)}$ and $\mathbf{b}_1$ with clear equivalents in the $Kr^+$ decay spectra (see Refs. [7, 14]). Based on our simulations the final states, which these lines represent, feature mixing with the $d$ orbital all the way to $9d$ in the case of Br*. The corresponding lines in $Kr^+$ feature this mixing to much lesser degree. The strong mixing can be attributed to the lower effective nuclear charge the electrons of Br* experience when compared to $Kr^+$. On the lower kinetic energy side of the linegroup $\mathbf{b}_1$ at around 20 eV we see an increasing background with few barely distinguishable features. Our calculations however predict the existence of two intense peaks, which we have labeled **a**, at around the 10 eV in Fig. 2. The peaks can be seen in the dotted line representing the simulated decay without the contribution from the subsequent decay to the widths. This apparent discrepancy between the measured and predicted spectra can be explained with the help of multielectron coincidence studies as discussed in the following subsection.

### B. Subsequent Auger decay and double photoionization in Br

The $j = 5/2$ component of the double photoionization (DPI) spectrum following the $3d \rightarrow \sigma^*$ resonance has been extracted from the collected Auger electron-Auger electron coincidence map in Fig. 1 by integrating diagonally along the total excess energy. Comparison with the double photo ionization spectrum measured off the resonance is presented in the (iv) frame of Fig. 1.

The collected electron-electron energy correlation map measured at resonance in Fig. 1 reveals thin diagonal lines associated with the atomic Br$^2$+ states as well as broad bands due to molecular valence double ionization. The $Br^{2+}$ lines represent the final states of the two-step Auger decay cascade process starting from the Br* $3d_{5/2}^{-1}$ hole state. The double photoionization (DPI) spectrum measured on the $3d_{5/2} \rightarrow \sigma^*$ resonance in the (iv) frame of Fig. 1 is obtained via integration along the direction of these diagonal lines and feature three distinct linegroups. In the binding energy range from about 26 eV

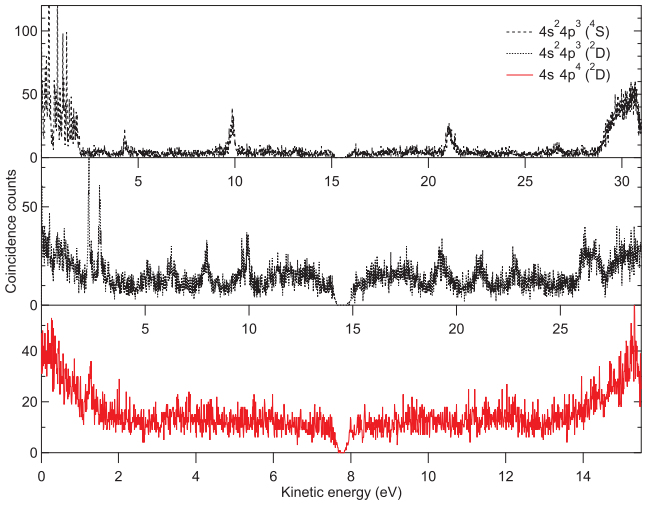


FIG. 3. Energy sharing between the two Auger electrons emitted in the two-step Auger decay cascade of the Br $3d_{5/2}^{-1}$ hole and populating respectively the $Br^{2+}4s^24p^3$ ($^2D$), ($^4S$) or $4s14p4$ ($^2D$) final states (see the frame (v) of Fig. 1). These spectra are obtained from the intensities along the diagonal lines in Fig. 1 and presented in kinetic energy of the corresponding slow electron.

to 33 eV one can observe wide lines resulting from the HBr molecule. These peaks can be seen also in the off-resonance spectrum measured at $h\nu = 75.3\ eV$ and they form its only noticeable feature.

The binding energy range from about 33 eV up to 39 eV in the (v) frame of Fig. 1 features three prominent lines with few minor peaks between and partially under them. According to our simulation the features in this region result from the decay into $Br^{2+}$ states, which have the configuration $4s^24p^3$ as the main contributor. These lines appear only when measured on the resonance channel as they get populated as the energetically possible intermediate $Br^+$ states decaying via normal Auger process.

The peak seen at 49 eV in the (v) frame of Fig. 1 and its lesser companion at 46 eV correspond to doubly ionized states with the configuration $4s4p^4$ as the main contributor. According to our theoretical calculations this intense line at 49 eV corresponds to the final state of the Auger decay, of which initial $Br^+$ state ($4p^6$ as the main contributor thus labeled **a**) can be seen in the calculated spectrum in Fig. 2 at about 10 eV. As already mentioned earlier, the corresponding peak is not seen in the measured spectrum. This discrepancy can be understood by utilizing coincidence measurements. From the map in Fig. 1 it is possible to see that the diagonal constant total excess energy line, which gives arise to the observed peak at the 49 eV in the two-dimensional projection, has electron counts distributed rather evenly along its length. This can also be observed from the kinetic energy sharing diagrams in Fig. 3, which reveal the U-shaped intensity distribution of the line at 49 eV, namely $4s4p^4$ ($^2D$),

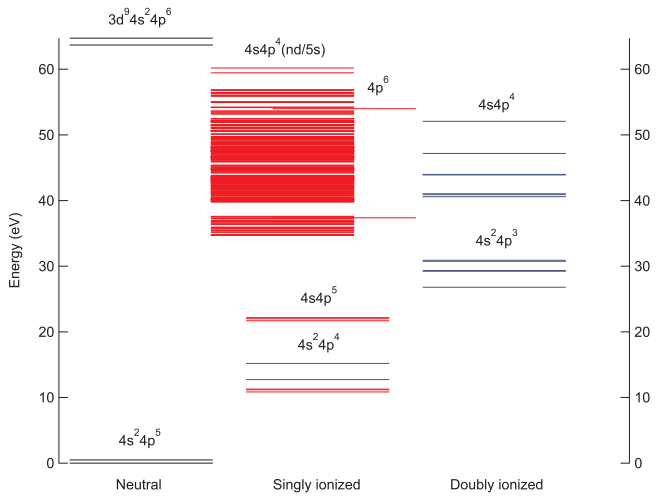


FIG. 4. The energy level diagram showing the energies of some selected atomic states of neutral, singly, and doubly ionized atomic bromine relative to the energy of the ground state. Each horizontal line represents an individual state and has been placed under the label of its major contributing electron configuration.

whereas the other lines feature sharp peaks, which correspond to the singly ionized, intermediate $Br^+$ states.

The usual cause for such U-shaped distribution is a direct double photoionization, which however can be ruled out here, since the peak does not appear in the spectrum collected off resonance (see frame (iv) of Fig. 1). In this case such behavior is best explained by the initial $Br^+$ state of the Auger decay having an extremely short lifetime. This interpretation is consistent with the collected data and the theoretical predictions; in the simulation of the subsequent $N_1N_{2,3}N_{2,3}$ super Coster-Kronig type decay the initial $Br^+$ states (at around 10 eV in Fig. 2) decay very fast into their final $Br^{2+}$ states causing extreme broadening of the lines making them effectively disappear into the background. Our calculations predict a width of at least 12 eV, which means that the intermediate $4p^6$ state has a lifetime of only 28 as. This explains why the peaks are not distinguishable from the measured spectra and also the even distribution along the observed diagonal in the coincidence map of Fig. 1 and the U-shaped diagram in Fig. 3. The energy level diagram in Fig. 4 shows, how close in energy this short-lived, intermediate $Br^+$ $4p^6$ state is to the final state of the decay namely $Br^{2+}$ $4s4p^4$. The main contributing configuration $4p^6$ of the intermediate state readily mixes with $4s4p^4(5s, nd)$ $(n = 4, 5, 6, 7, 8, 9)$. The final state $4s4p^4\epsilon\ell$, in which $\epsilon\ell$ denotes the ejected electron in the continuum, can be thought as a continuation of this trend thus providing further credibility for the short lifetime of the intermediate $Br^+$ state.

### C. Evolution of spectral features in the isoelectronic series Br, Kr, and Rb

The collected Auger spectra resulting from the decay of $3d_{5/2}^{-1}4s^24p^6$ hole state in the cases of atomic $Br^*$, $Kr^+$, and $Rb^{2+}$ are presented as solid lines (blue) in the upper panels of their respective frames in Fig. 5. The lower panel of each frame shows the corresponding spectra (in red) simulated with FAC. The labeling scheme follows the one established for $Br^*$ in Fig. 2.

The present identifications of the peaks in $Kr^+$ spectrum are in agreement with the studies by Partanen [14] and Paladoux [7], though it should be noted that the main contributing configurations are not always identical. This discrepancy can however be attributed to the atomic states in this energy region generally being sensitive to configuration correlation. The effect can be easily observed in Fig. 5 at around 40 eV with $\mathbf{d}/\mathbf{c}_1$ linegroup, which has a fairly simple structure and can be reproduced in computations even with a single-configuration calculation including the $4s4p^5$ ($\mathbf{d}$) configuration. In the multi-configuration run $4s4p^5$, however, is not the leading configuration for all the lines in the group throughout the isoelectronic series as it readily mixes with $4s^24p^34d$. Regardless the overall shape and intensity distribution are similar between single-configuration and multi-configuration calculations.

The $3d$ Auger decay spectra of all the atoms in the isoelectronic series resemble each other to such degree that it is possible to visually identify the corresponding linegroups in the kinetic energy range from approximately 10 to 60 eV. We observe certain trends in Fig. 5 when moving from $Br^*$ to $Rb^{2+}$. One such trend is the structure of the spectrum being richest in the case of $Br^*$ and becoming simpler with $Kr^+$ and $Rb^{2+}$. The presence of the HBr molecular lines in our collected $Br^*$ spectrum makes the visual comparison somewhat challenging, but the kinetic energy range, in which this trend is most easily observable, lies below 37 eV and does not show any molecular lines. The linegroup $\mathbf{c}_1/\mathbf{c}_{2x}$, which in $Br^*$ spectrum can be found between 30 and 37 eV, lies at lower kinetic energies between 26 and 32 eV in the case of $Kr^+$ and between 25 and 30 eV in $Rb^{2+}$. According to our calculations the group also features reduced contribution from configurations in which $nd$ orbital $(n = 5 \ldots 9)$ is singly occupied. This contribution gives the group its complex structure in the $Br^*$ case. On the lower kinetic energy side of this group we see groups labeled $\mathbf{a}(\mathbf{b}_2)/\mathbf{b}_2$, $\mathbf{c}_1/\mathbf{c}_{5d}$ (absent in $Kr^+$), and $\mathbf{b}_1$ in the order of descending kinetic energy. The most intense peak in the $\mathbf{b}_2$ group at around 21 eV in the measured $Rb^{2+}$ spectrum seems to be split in two, a feature not reproduced in our spectrum simulated with FAC. The discrepancy will be discussed later in this section.

We can also see from Fig. 5 that with the exception of linegroups highest in kinetic energy $\mathbf{e}$ $(4s^24p^4)$ and $\mathbf{d}(\mathbf{c}_1)$ $(4s4p^5)$, all the groups move towards lower kinetic energies as the atomic number increases within the iso-

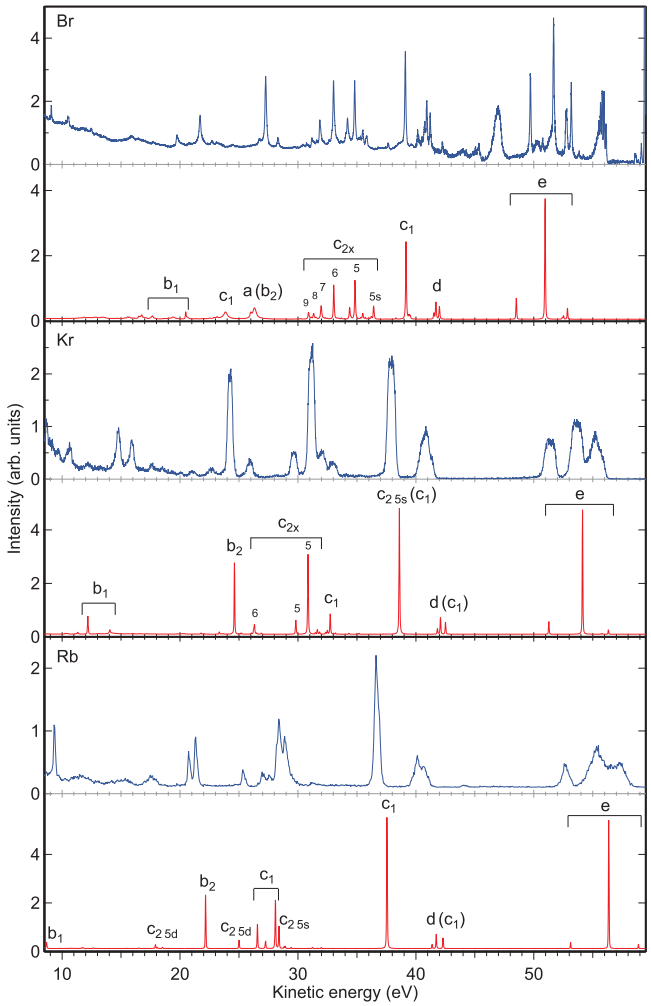


FIG. 5. The measured and simulated Auger spectra resulting from the decay of the $3d_{5/2}^{-1}$ state presented in the emboldened frames for Br, Kr, and Rb respectively. In each frame the upper panel (blue) depicts the collected spectrum whereas the lower (red) shows the results of the theoretical simulation with the contribution of the subsequent Auger decay to the width added. Labels correspond to the different contributing configurations in the following manner; **a**: $4p^6$, $\mathbf{b}_1$: $4s4p^4(5s, 6/7/9d)$, $\mathbf{b}_2$: $4s4p^44d$, $\mathbf{c}_1$: $4s^24p^34d$, $\mathbf{c}_{2x}$: $4s^24p^3(5s, nd)$, **d**: $4s4p^5$, **e**: $4s^24p^4$. Bracketed labels correspond to configurations that strongly mix with the main contributing configurations. In the case of $\mathbf{c}_{2x}$ additional $n/n\ell$ labeling marked as subscript in the place of $x$ or above the corresponding peaks defines the configuration in more detail.

electronic series. Group **e** moves towards higher energy and the location of $\mathbf{d}(\mathbf{c}_1)$ seems to stay relatively constant. The recorded kinetic energies of the ejected Auger electron represent differences in binding energy between between the initial and various final states of the first step of the decay. A selection of such states is presented as an energy level diagram in Fig. 4 for Br*. By looking at the diagram one can get an idea on how its overall shape changes as a function of $Z$. From the aforementioned trends within the isoelectronic series in Fig. 5 we can see that as $Z$ increases the states characterized by configuration $4s^24p^5$ (group **e** in Fig. 5) move further away (downwards in Fig. 4) from the the initial $3d^{-1}$ state, whereas the energy difference between the initial and the $4s4p^5$ states remains almost constant. The states dominated by the other included configurations such as $4p^6$, $4s4p^4(nd/5s)$, and $4s^24p^3(nd/5s)$ (labels **a**, $\mathbf{b}_1/\mathbf{b}_2$, and $\mathbf{c}_1/\mathbf{c}_{2x}$ in Fig. 5 respectively) move closer to the initial hole state as $Z$ increases.

The reason for such opposite behavior of different intermediate states relative to the initial $3d^{-1}4s^24^6$ hole state can be attributed to how strongly the energy of each state is affected by an increase in the effective nuclear charge experienced by the electrons of interest as we move from Br* to $Kr^+$ and $Rb^{2+}$. The atomic states that shift towards lower energies or stay approximately the same relative to the initial $3d$ hole state as the atomic number $Z$ increases are dominated by configurations $4s^24p^4$ (**e**) and $4s4p^5$ (**d**) respectively. The states in which the leading configuration is $4p^6$ (**a**) or has $nd/5s$ ($n = 4 \ldots 9$) singly occupied move closer the $3d$ hole state in energy (upwards in Fig. 4). From this one can see that the increasing effective nuclear charge has a stronger binding effect on the energies of $4s^24p^4$ and $4s4p^5$ states than on other states. The electrons in $s$-subshells are in general more sensitive than those on other subshells to the changes in the nuclear charge.

Based on our calculations the final states of the second step decay become more loosely bound (move up in Fig. 4) in heavier elements of the series thus causing more and more channels that can populate the $4s^24p^3$ and $4s4p^4$ states in the case of Br* to become energetically unavailable in $Kr^+$ and $Rb^{2+}$. This is why we can observe the fast decay between states described by configurations $4p^6$ and $4s4p^4$ respectively only in Br*. The increased separation in energy between the intermediate and final states also decreases the probability of configuration correlation, which we can observe as a simpler spectral structure in the heavier counterparts of Br* $3d$ hole decay.

The seemingly split peak in $Rb^{2+}$ $3d$ hole decay spectrum at about 21 eV in the measured spectrum in Fig. 5 is not reproduced in the calculations with FAC. The supplementary simulation with GRASP2K presented in the middle panel of Fig. 6 however reproduces this double-peak structure at about 24 eV in kinetic energy. According to the interpretation based on this calculation we are actually not observing a split peak, but instead two individual lines originating from decays into states of opposite parity. We have identified the line lower in kinetic energy as $4s4p^44d$ ($\mathbf{b}_2$) earlier in this section. The equivalent of this line can be found throughout the studied isoelectronic series as can be seen from Fig. 5. The GRASP2K simulation suggests that the leading configuration of this state is $4p^6$ (**a**) with $4s4p^44d$ ($\mathbf{b}_2$) having the second largest contribution. This difference between the two simulations further demonstrates the sensitivity

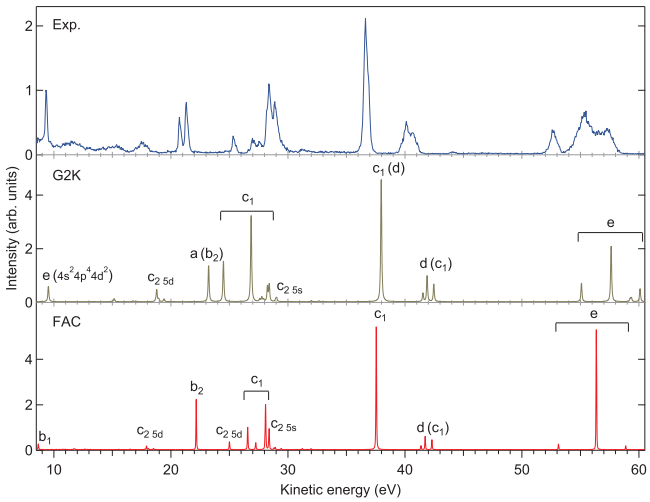


FIG. 6. Comparison of the measured Auger spectrum resulting from the decay of the $Rb^{2+}$ $3d_{5/2}^{-1}$ state with the spectrum simulated using GRASP2K (brown) and flexible atomic code (red) presented in kinetic energy. Labels correspond to the different contributing configurations in the following manner; **a**: $4p^6$, $\mathbf{b}_1$: $4s4p^4(5s, 6/7/9d)$, $\mathbf{b}_2$: $4s4p^44d$, $\mathbf{c}_1$: $4s^24p^34d$, $\mathbf{c}_{2x}$: $4s^24p^3(5s, nd)$, **d**: $4s4p^5$, **e**: $4s^24p^4$. Bracketed labels correspond to configurations that strongly mix with the main contributing configurations. In the case of $\mathbf{c}_{2x}$ additional $n/n\ell$ labeling marked as subscript in the place of $x$ defines the configuration in more detail.

of simulations of these atomic states to the effects of configuration correlation. The other peak right on the higher kinetic energy side of the one just discussed seems to be absent in the FAC simulation, but based on calculations with GRASP2K it can be assigned $4s^24p^34d$ ($\mathbf{c}_1$). This makes the peak a part of the linegroup stretching from 24 to 29 eV and defined by $\mathbf{c}_1/\mathbf{c}_{2x}$ in the middle panel of Fig. 6. This interpretation means that these two lines just happen to appear at almost the same energy manifesting as something that with a quick glance looks like a split peak. The simulation run with FAC consists of a larger set of configurations so it is likely that the higher kinetic energy line is not truly absent but only seems like it because it does not receive enough intensity. The observation visually evident in Fig. 6, in which the overall intensity distribution given by GRASP2K seems to better match the collected spectrum, hints towards this conclusion. A comparison of individual atomic states of these two calculations would however not be meaningful due to different set of configurations used for the runs. The more limited configuration set used in GRASP2K seems to be able to reproduce the decay spectrum in the case of $Rb^{2+}$ due to the reduced configuration interaction compared to the lighter isoelectronic counterparts, of which electrons experience a lower effective nuclear charge. For the lighter ones the large set used in FAC yields better results.

## V. CONCLUSIONS

The Auger decay following the $3d$ hole state in the electron configuration $3d^{-1}4s^24p^6$ was studied using synchrotron radiation and recorded with a magnetic bottle setup as a coincidence experiment for the isoelectronic series of $Br^*$, $Kr^+$, and $Rb^{2+}$. The resonant $Br^*$ decay spectrum was recorded also with a hemispherical energy analyzer in higher resolution. Interpretation of the results was done with the aid of MCDF calculations. A good agreement between the measurements and theoretical predictions was reached, which enabled us to identify the lines visible in the $Br^*$ resonant Auger decay spectrum and interpret the corresponding coincidence map as well as discover trends in spectral features within the studied isoelectronic series.

The $Br^*$ resonant Auger decay (first step) was found to be followed by a very fast super-Coster-Kronig type $NNN$ Auger decay (second step), which broadens one of the lines in the first-step decay spectrum into the background. An increased contribution of electron configurations, in which $nd$ ($n = 4 \ldots 9$) subshell is singly occupied, was observed in $Br^*$. The strength of configuration interaction was found to be inversely proportional to the atomic number $Z$ within the isoelectronic series. This and the observed evolution of the energies of different corresponding states within the series could be attributed to the increased effective nuclear charge experienced by the electrons of interests as $Z$ increases.

## ACKNOWLEDGMENTS

We are grateful to R. Püttner for his help during the measurements and to the BESSY and UVSOR staff for the stable operation of the synchrotrons during these measurements. This work has been financially supported in part by the European Community, Research Infrastructure Action under the FP6 "Structuring Eurepoean reserch Area" Programme (contract R II 3-CT-2004-506008) and by the Research Council for Natural Sciences and Engineering of the Academy of Finland. P.L. acknowledges the support of the Institute of Molecular Science and J.K. acknowledges EXACTUS-DP (Doctoral Program in Exact Sciences), the Magnus Ehrnrooth foundation, and Vilho, Yrjö and Kalle Väisälä fund.

[1] P. Auger, J. Phys. Radium **6**, 205 (1925)

[2] T. A. Carlson and M.O. Krause, Phys. Rev. Lett. **14**, 390 (1965)

[3] T. A. Carlson and M.O. Krause, Phys. Rev. Lett. **17**, 1079 (1966)

[4] P. Lablanquie, S. Sheinerman, F. Penent, R.I. Hall, M. Ahmad, Y. Hikosaka, and K. Ito, Phys. Rev. Lett. **87**, 053001 (2001)

[5] J. Viefhaus, S. Cvejanović, B. Langer, T. Lischke, G. Prümper, D. Rolles, A. V. Golovin, A.N. Grum-Grzhimailo, N.M. Kabachnik, and U. Becker, Phys. Rev. Lett. **92**, 083001 (2004)

[6] F. Penent, J. Palaudoux, P. Lablanquie, L. Andric, R. Feifel, and J.H.D. Eland, Phys. Rev. Lett. **95**, 083002 (2005)

[7] J. Palaudoux, P. Lablanquie, L. Andric, K. Ito, E. Shigemasa, J. H. D. Eland, V. Jonauskas, S. Kučas, R. Karazija, and F. Penent, Phys. Rev. A **82**, 043419 (2010)

[8] A.G. Kochur, V.L.Sukhorukov, A.J. Dudenko, and P.V. Demekhin, J. Phys. B At. Mol. Opt. Phys. **28**, 387 (1995)

[9] J. Zeng, P. Liu, W. Ziang, and J. Yan, Phys. Rev. A **87**, 033419 (2013)

[10] P. Lablanquie, M.A. Khalal, L. Andric, J. Palaudoux, F. Penent, J.-M. Bizau, D. Cubaynes, K. Jänkälä, Y. Hikosaka, K. Ito, K. Bučar, and M. Žitnik, J. Electron Spectrosc. Relat. Phenom. **220**, 125 (2017)

[11] W. Mehlhorn, Z. Physik **187**, 21 (1965)

[12] H. Aksela, S. Aksela, and H. Pulkkinen, Phys. Rev. A **30**, 2456 (1984)

[13] J. Jauhiainen, H. Aksela, S. Aksela, A. Kivimäki, O.-P. Sairanen, E. Nõmmiste and J Végh, J. Phys. B **28**, 3831 (1995)

[14] L. Partanen, M. Huttula, H. Aksela and S. Aksela, J. Phys. B **40**, 3795 (2007)

[15] V. Jonauskas, R. Karazija and S Kučas, J. Phys. B **41**, 215005 (2008)

[16] M. Mazzoni and M. Pettini, Phys. Lett. A **35**, 330 (1981)

[17] A. Cummings and G. OSullivan, Phys. Rev. A **54**, 323 (1996)

[18] L. Nahon, P. Morin, and F. Combet-Farnoux, Phys. Scr. **1992**, 104 (1992)

[19] P. and I. Nenner, Phys. Rev. Lett. **56**, 1913 (1986).

[20] P. Lablanquie, H. Iwayama, F. Penent, K. Soejima, and E. Shigemasa, J. Electron Spectrosc. Relat. Phenom. **195**, 96 (2014)

[21] X.-J. Liu, Q. Miao, F. Gelmukhanov, M. Patanen, O. Travnikova, C. Nicolas, H. Ågren, K. Ueda, C. Miron, Nat. Photonics **9**, 120125 (2014).

[22] S.-M. Huttula, P. Lablanquie, L. Andric, J. Palaudoux, M. Huttula, S. Sheinerman, E. Shigemasa, Y. Hikosaka, K. Ito, and F. Penent, Phys. Rev. Lett. **110**, 113002 (2013).

[23] M. A. Khalal, P. Lablanquie, L. Andric, J. Palaudoux, F. Penent, K. Bučar, M. Žitnik, R. Püttner, K. Jänkälä, D. Cubaynes, S. Guilbaud, and J.-M. Bizau, Phys. Rev. A **96**, 013412 (2017).

[24] K. J. S. Sawhney, F. Senf, M. Scheer, F. Schäfers, J. Bahrdt, A. Gaupp, and W. Gudat, Nucl. Instrum. Methods Phys. Res. A **390**, 395-402 (1997).

[25] M. F. Gu, Can. J. Phys. **86**, 675-689 (2008)

[26] F. A. Parpia, C. Froese Fischer, and I. P. Grant, Comput. Phys. Commun. **94**, 249 (1996).

[27] P. Jönsson, X. He, C. Froese Fischer, and I. P. Grant, Comput. Phys. Commun. **177**, 597 (2007).

[28] S. Fritzsche, J. Electron Spectrosc. Relat. Phenom. **114-116**, 1155 (2001).

[29] S. Fritzsche, Comput. Phys. Commun. **187**, 1525-1559 (2012).